remote sensing

MDPI

Article

Calibrating Satellite-Based Indices of Burn Severity from UAV-Derived Metrics of a Burned Boreal Forest in NWT, Canada

Robert H. Fraser [1,*], Jurjen van der Sluijs [2] and Ronald J. Hall [3]

[1] Canada Centre for Mapping and Earth Observation, Natural Resources Canada, Ottawa K1S 5K2, ON, Canada
[2] Centre for Geomatics, Government of the Northwest Territories, Yellowknife X1A 2L9, NT, Canada; Jurjen_vanderSluijs@gov.nt.ca
[3] Canadian Forest Service, Natural Resources Canada, Edmonton T6H 3S5, AB, Canada; Ron.Hall@Canada.ca
* Correspondence: Robert.Fraser@Canada.ca; Tel.: +1-613-694-2621

Academic Editors: Diofantos Hadjimitsis, Ioannis Gitas, Luigi Boschetti, Kyriacos Themistocleous and Prasad S. Thenkabail
Received: 9 February 2017; Accepted: 13 March 2017; Published: 16 March 2017

Abstract: Wildfires are a dominant disturbance to boreal forests, and in North America, they typically cause widespread tree mortality. Forest fire burn severity is often measured at a plot scale using the Composite Burn Index (CBI), which was originally developed as a means of assigning severity levels to the Normalized Burn Ratio (NBR) computed from Landsat satellite imagery. Our study investigated the potential to map biophysical indicators of burn severity (residual green vegetation and charred organic surface) at very high (3 cm) resolution, using color orthomosaics and vegetation height models derived from UAV-based photographic surveys and Structure from Motion methods. These indicators were scaled to 30 m resolution Landsat pixel footprints and compared to the post-burn NBR (post-NBR) and differenced NBR (dNBR) ratios computed from pre- and post-fire Landsat imagery. The post-NBR showed the strongest relationship to both the fraction of charred surface (exponential R^2 = 0.79) and the fraction of green crown vegetation above 5 m (exponential R^2 = 0.81), while the dNBR was more closely related to the total green vegetation fraction (exponential R^2 = 0.69). Additionally, the UAV green fraction and Landsat indices could individually explain more than 50% of the variance in the overall CBI measured in 39 plots. These results provide a proof-of-concept for using low-cost UAV photogrammetric mapping to quantify key measures of boreal burn severity at landscape scales, which could be used to calibrate and assign a biophysical meaning to Landsat spectral indices for mapping severity at regional scales.

Keywords: forest fire; burn severity; composite burn index; normalized burn ratio; unmanned aerial vehicle; UAV; UAS; Landsat

1. Introduction

Wildfires are a major cause of disturbance in North American boreal forests, burning an annual average of approximately 10,000 km^2 in the 1960's and more than 31,000 km^2 in the 1990's [1]. There is high interannual variability in the area burned [2], and boreal fires can exert a considerable influence on the species composition, diversity, and stability of many forest ecosystems [3]. Fires can cause large fluxes of carbon within an ecosystem [4] and release a tremendous quantity of carbon to the atmosphere [5]. This can lead to a boreal forest becoming a significant net carbon source, particularly when combined with severe insect disturbances [2]. The near-complete mortality of forest vegetation after boreal fires in North America has modified wildlife habitats, including the elimination of lichen that caribou forage upon [6]. In colder permafrost environments, the active layer depth also often shows a

long-term increase after a fire, due to the removal of the insulating surface organic layer [7]. Of particular concern is the projected increase in the area, frequency, and severity of fire under a changing climate, and its potential to exacerbate changes in vegetation succession and ecosystem function [8–10].

Burn severity is a term used to describe the magnitude of ecological change caused by fire [11]. Knowledge of burn severity is important for predicting the post-fire vegetation community [12], assessing the availability of residual seed sources to promote regrowth [13], predicting long-term forest successional patterns [13], and determining changes in bird abundance [14]. Boreal burn severity has been assessed in North America using a variety of methods that span spatial scales from plot measurements [15–17], to high resolution air photos [18], airborne hyperspectral imagery [19], airborne Lidar [20], and satellite imagery for mapping at landscape to regional scales [21].

A commonly applied field method for assessing burn severity in forests is the Composite Burn Index (CBI) [22]. The CBI provides a numerical index of vegetation damage from fire by integrating visual estimates of damage, stratified by five vertical layers (substrate, herbs and low shrubs < 1 m, tall shrubs and saplings 1–5 m, sub-canopy trees, and canopy trees), using a scale of 0 (unchanged) to 3 (high severity). The CBI provides a rapid means of assessing burn severity that integrates a variety of ecologically significant burn severity indicators. Some limitations and challenges in applying the CBI include: (1) the qualitative nature of its assessments, which could vary among observers [23]; (2) the difficulty and cost involved in accessing remote burn sites on the ground; (3) the potentially large number of plots required to represent the range of conditions in a large, heterogeneous burned area; (4) a need to infer pre-fire fuel conditions for assessing consumption and mortality [23]; and (5) a limited ability to quantify organic layer consumption [24], which is an important measure of severity in northern boreal forests. Despite these limitations, the CBI is a widely used field method in burn severity assessment [23].

A wide range of satellite-based approaches have also been developed to map burn severity over larger forested areas [11,25,26]. A common method is to compute the difference between the pre-fire and post-fire Normalized Burn Ratio (NBR), which is based on the near-infrared and shortwave infrared bands from 30 m resolution Landsat imagery [21,22]. The difference in the NBR (dNBR) has been effective for mapping burn severity in Canadian forests [16,27,28], but less so for Alaskan spruce forests [29,30], where the severity strongly depends on the depth of burning in the surface layer [29]. Since dNBR only measures a spectral response change, it is the calibration with the plot-based CBI that provides the ability to transform larger-area dNBR values into maps of varying burn severity [22]—an approach that has been applied across different regions of boreal forest [21]. For example, a non-linear relationship between CBI and dNBR was derived for several boreal fires within Western Canada, by Hall et al. [16]. Some considerations for applying this CBI-Landsat calibration approach include: (1) the requirement to identify CBI plots that should be relatively homogeneous at a 90 m, 3-by-3 Landsat pixel scale; (2) the need for cloud-free, post-burn Landsat imagery that closely matches the CBI sampling date; and (3) an understanding of the complex physical relationship between CBI's multiple, integrated measures of severity and spectral changes, measured using satellite-based indices [11,23,31].

Driven by a need to acquire highly detailed information over larger areas, relative to field plots, unmanned aerial vehicles (UAVs) have been growing in popularity as a means of conducting inexpensive, on-demand remote sensing that can bridge measurement scales between field plots and satellite imagery [32]. While there have been a number of applications of thermal sensors on UAVs to map actively burning fires [26], there has been a limited use of UAVs for assessing vegetation burn severity. One application involved the use of a multispectral imager mounted on a large, military-grade UAV system, to generate NBR maps in the Western US [33]. More recently, a post-fire digital terrain model (DTM) derived from a UAV survey was differenced with a pre-fire DTM from airborne LiDAR, to estimate the depth of surface burning in a tropical peatland [34]. The purpose of our study was to assess the potential for using a small, multicopter UAV to map indicators of boreal forest burn severity at landscape scales, and to up-scale this information to calibrate Landsat spectral indices, thus representing biophysically meaningful measures of severity over larger areas. As a result, we

also conducted a limited comparison of plot-based CBI values with both UAV and Landsat indices of burn severity.

2. Materials and Methods

2.1. Study Area and Fires

This study was conducted 120 km southwest of Yellowknife, NWT, Canada, at three sites within 3 km of each other that burned during summer 2014 (Figure 1). The affected forest lies within the Great Slave Plain High Boreal Ecoregion, which contains closed to open canopy stands of pure and mixed tree species, comprising jack pine (*Pinus banksiana* Lamb.), white spruce (*Picea glauca* (Moench) Voss), black spruce (*Picea mariana* (Mill) B.B.P.), and trembling aspen (*Populus tremuloides* Michx.) [35]. A widespread fire outbreak occurred in NWT in 2014, during extreme fire danger conditions that affected 3.4 million ha of forest lying primarily in the region surrounding Yellowknife. CBI plot measurements collected by the Canadian Forest Service and Government of NWT at select burned sites (n = 54) in the larger region, had an average combined CBI score of 2.03, indicating a moderate-to-high average burn severity. These plots were surveyed in summer 2015 and 2016, according to the methods described in Hall et al. [16]. Similar to [36], we believe that the sampling of some sites two years after the fire did not negatively impact our ability to determine burn severity in this moderate-to-high severity burn. The CBI estimates of both years were combined into a single dataset for analysis with the remote sensing indices. We used UAV and satellite sensor data collected in the summer following burning to provide an extended assessment of severity that accounted for delayed mortality and early vegetation regeneration [22].

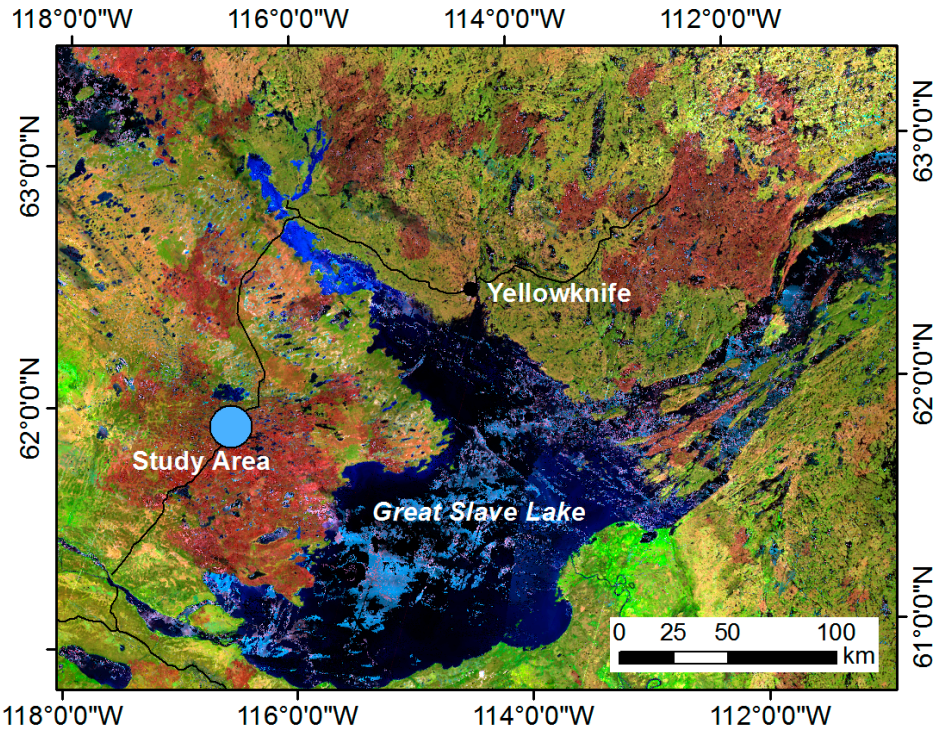

Figure 1. Location of study area in Northwest Territories (blue circle) showing the extent of regional burning in 2014 (dark red patches), visible in a Proba-V satellite image composite from September 2014.

2.2. UAV Imagery and Processing

UAV-based photographic surveys of the burned study sites were conducted on the 4–5 August 2015 using a PX8 octocopter developed by Xpedition Robotics. This octocoper carried the Pixhawk flight

controller running Arducopter 3.2 software and a 24 megapixel Sony a6000 mirrorless camera with a 20 mm Sony pancake lens. Mission Planner software was used to plan autonomous flights at 90 m above ground level in a grid pattern, to capture nadir imagery with ~2 cm resolution (Figure 2), 85% forward overlap, and 68% side overlap. Three separate burned sites containing a range of severities and fuel types were surveyed (Table 1). A recent forest inventory by the Government of NWT, based on 2013 air photos, was used to identify the dominant pre-burn tree species within each survey area.

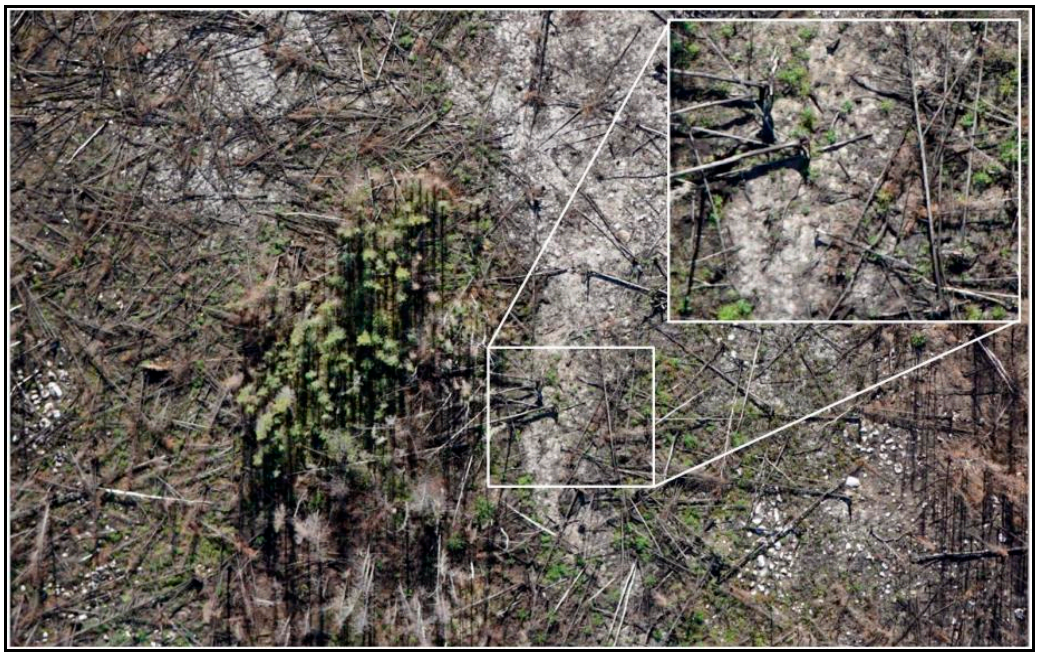

Figure 2. Portion of a 24 megapixel photo taken over survey area #3 using a Sony a6000 camera mounted to an octocopter UAV. Portions of the fire completely consumed the surface organic layer, exposing the bright underlying mineral soil.

Table 1. Details of the 2014 burned sites surveyed using an octocopter UAV in early August, 2015. The dominant tree species are listed in decreasing order of percent cover, where Sw = white spruce, Sb = black spruce, A = trembling aspen, and Pj = jack pine.

Survey ID	Surveyed Area (ha)	# UAV Photos	# 30 m Landsat Pixels	# Forest Inventory Units	Dominant Tree Species	# CBI Plots (2015, 2016)
1	49.7	1401	462	12	Sw, Sb, A	3, 24
2	9.3	285	66	2	Pj	1, 7
3	10.1	280	77	5	Pj, Sw, Sb	1, 3

The highly overlapping UAV photos were processed into dense 3D point clouds, 3 cm resolution digital surface models (DSMs), and 3 cm resolution colour orthomosaics, using Pix4d mapper v2.0 software. Pix4d uses proprietary Structure from Motion (SfM) algorithms in an automated workflow to match common features (keypoints) between corresponding images, apply a photogrammetric bundle adjustment, and create dense 3D point clouds using multiview stereo matching [37]. The specific settings used for Pix4d point cloud generation were: a half image-scale, optimal point density, and a minimum of two matches, which resulted in point cloud densities of about 200 points per m^3. The point clouds were used in Pix4d to create DSMs representing the upper surface of all scene features, which could then be applied to ortho-rectify and mosaic the photos, thus generating orthomosaics. LAStools software was used to denoise and classify the point clouds into ground and non-ground objects, before triangulating and then rasterizing the ground points into a bare earth (or digital terrain) model. The heights of non-ground objects (e.g., all shrubs, dead-standing boles, green canopies)

were normalized, relative to the bare earth elevations (e.g., mineral soil, scorched moss, completely horizontal deadfall), which were subsequently triangulated and rasterized into a vegetation canopy height model that represents the heights of all objects above ground level.

We focussed on two basic indicators of burn severity (residual green vegetation and charred organic surface) that could be readily separated using UAV-based colour photographs and are known to have a strong relationship to remotely sensed reflectance [19,38]. These UAV-based indicators are also analogous to the subset of CBI factors that measure the surface duff condition (i.e., charring), the frequency of surviving vegetation, and the percentage of unaltered crown foliage [22]. Several visible-channel spectral indices were computed from the UAV orthomosaic digital numbers [39] (Table 2), to classify charred surface and green vegetation, which may represent either residual unburned moss and other vegetation, or early regeneration one year after a fire. A reference sample representing burned areas (100 polygons containing 5311 pixels), and green ground and tree canopy vegetation (100 polygons containing 3792 pixels), was manually digitized within the largest survey region (#1), with the aid of the raw 2 cm resolution UAV photos and ground photos from three CBI plots. These samples were used to compare the effectiveness of the different UAV indices for separating green vegetation.

2.3. Satellite Imagery and Processing

Pre- and post-fire 30 m resolution Landsat-8 images were used to compute the post-fire NBR (post-NBR) and the differenced Normalized Burn Ratio (dNBR) [22] (Table 2). Two Level-1T images from Path 48 Row 17 were acquired from USGS GloVis for 17 July 2013 and 23 July 2015, that provided near-anniversary, cloud- and smoke-free coverage of the surveyed sites. Radiance values were calibrated and converted to top-of-atmosphere reflectance channels using USGS coefficients following [40], and these were used to compute the burn severity indices.

Table 2. Description and formulation of UAV burn severity spectral indices, UAV burn severity indicators derived from the UAV indices, and Landsat spectral burn severity indices investigated in this study. NIR refers to Landsat's near infrared channel and SWIR2 refers to the second shortwave infrared channel centered at 2.2 μm.

Burn Severity Indices and Attributes	Channel Combination/Description
UAV spectral indices	
Excess Greenness (ExG)	$2G - R - B$
Normalized Greenness (NormG)	$G/(R + G + B)$
Normalized Green-Red Ratio (NormG-R)	$(G - R)/(G + R)$
Brightness	$R + G + B$
Maximum RGB Difference (MaxDiff)	$\text{Max}(\lvert B - G \rvert, \lvert B - R \rvert, \lvert R - G \rvert)$
Char Index (CI)	Brightness + (MaxDiff × 15)
UAV burn severity indicators	
Green Vegetation	From thresholding ExG index
Green Crown Vegetation	Green Vegetation above 5 m
Charred Surface	From thresholding Char Index
Landsat spectral indices	
Normalized Burn Ratio post-fire (post-NBR)	$(NIR - SWIR2)/(NIR + SWIR2)$
Differenced NBR (dNBR)	$NBR_{preburn} - NBR_{postburn}$

2.4. Data Analysis

The first three UAV spectral indices in Table 2 were assessed for their ability to discriminate green vegetation from all other surface types, using a simple statistic (S) that provided a measure of the index signal-to-noise ratio. A value greater than 1 indicates that the standard deviations of an

index for separating burned surfaces and green vegetation do not overlap, allowing reasonable class separation [41].

$$S = |x_b - x_g| / s_b + s_g \quad (1)$$

where S = separability statistic, x_b = mean UAV index value from burned surfaces, x_g = mean UAV index value from green vegetation, s_b = standard deviation of index from burned surfaces, and s_g = standard deviation of index from green vegetation.

A simple Jenks classifier was applied to the spectral index that provided the highest separability, to create a binary burned/green vegetation map. The Jenks classifier determined a class break value that produced two natural groupings by minimizing each class's average deviation from its mean, while maximizing each class's deviation from the other class's mean.

A new UAV-based index called the Char Index was formulated, to highlight charred organic surfaces (Table 2). This is a composite index based on the observation that charred surfaces have a very low visible reflectance (quantified using a Brightness Index) and a flat visible reflectance spectrum that produces the characteristic lack of colour [42] (quantified using a Maximum RGB Difference Index or MaxDiff). A multiplier of 15 was applied to the MaxDiff term to give it a similar weighting in the additive index. A threshold value of the Char Index was derived interactively, using the UAV imagery as a reference to create a binary map of dark, charred surfaces. A tree shadow mask was applied to the index to exclude shadows, which also have low Char Index values. We found that shadows could be effectively separated from all other cover types, including the charred surface, when applying a two-class Jenks classifier to the red channel (Figure 3d).

The 3 cm resolution map of green vegetation derived using the optimal greenness index was aggregated within the footprints of overlapping 30 m resolution Landsat pixels, to compute a fraction of green vegetation cover (i.e., Green Fraction). Similarly, the charred vegetation classification was aggregated to derive a 30 m char fraction (i.e., Char Fraction). Of interest was a statistical comparison of the up-scaled UAV-based indicators of burn severity and the Landsat burn severity indices. The UAV vegetation canopy height model was also used to separate green tree crown vegetation (>5 m) in the binary green vegetation classification (i.e., Green Tree Fraction). It is worth noting that direct georeferencing of UAV photos using the onboard GPS typically provides 1–2 m accuracy in the generated orthomosaic [43], compared to 12 m CE90 registration accuracy for Level-1T Landsat-8 imagery. Therefore, co-registration of the two datasets should normally be within 14 m, or one-half of a Landsat pixel.

The 30 m pixels that comprised each of the three study areas (Table 1) were randomly partitioned into model calibration (70%) and validation (30%) data sets. These data sets were then compared using a two sample Kolmogorov-Smirnov test, to determine whether the empirical distribution functions were statistically similar [44]. Several non-linear regression functions were examined using Data-Fit, a curve fitting and data plotting software tool by Oakdale Engineering, to find the optimal model form of best fit throughout the range of data, for both post-dNBR and dNBR as predictors of the UAV burn severity indicators (i.e., by comparing the coefficient of multiple determination—adjusted R^2, root mean square error—RMSE, significance of model coefficients, simplicity of model form, and graphical plots of model functions). The selected model was applied to the validation data set, from which the predicted values were evaluated using the Wilcoxin signed-rank test to test for statistical differences at the 5% level of significance. Standardized residual plots using the validation sample were also constructed, to obtain insights into the distribution of the residuals over the range of post-dNBR and dNBR.

The binary, UAV-based maps of green vegetation, green crown vegetation, and charred surface, were also separately aggregated within the 30 m extents of the 39 of 54 CBI plots that were collected within the study burns. This allowed for a separate comparison of the UAV metrics and Landsat indices to the CBI burn severity scores, by again examining a range of non-linear regression functions.

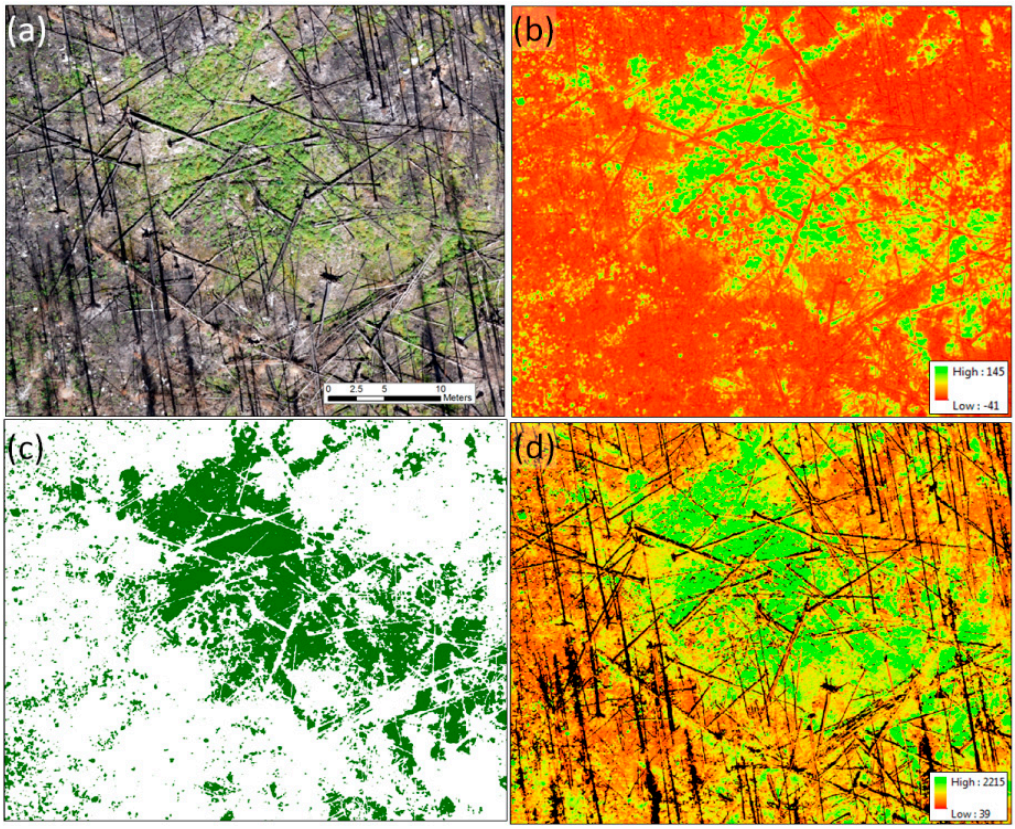

Figure 3. Portion of study area #1 showing (**a**) a 3 cm UAV photo-orthomosaic within study area #1 with burned and green vegetation; (**b**) the UAV Excess Greenness Index; (**c**) a binary classification of green vegetation derived from thresholding the Excess Greenness Index; and (**d**) the Char Index, where more highly charred areas with a low index value appear orange-red and masked tree shadows are shown in black.

3. Results

The separability statistic (S) derived for each UAV index indicated that the Excess Greenness (ExG) index (Figure 3b) provided the best discrimination of the burned and green vegetation samples (S = 2.2), followed by NormG (S = 1.9) and NormG-R (S = 1.0). We therefore applied the binary classifier to ExG and assessed the resulting map accuracy (Figure 3c) using the reference samples. The natural breaks (Jenks) classification produced a very high accuracy, with only 68 of 5268 (1.3%) burned samples and 5 of 3794 (0.13%) unburned samples being classified incorrectly. This high accuracy is the result of the two classes' ExG mean values being separated by more than two standard deviations (S = 2.2), and the fact that reference samples were selected with a relatively high confidence and did not include borderline cases, such as partially scorched crowns.

The two-sample Kolmogorov-Smirnov test indicated that the probability distributions of UAV and Landsat index values from the model calibration (70%) and validation (30%) datasets were significantly similar (p-values 0.32–0.64). A non-linear, exponential function in the form $Y = ab^x$ was found to be suitable for modeling the relationships between the two Landsat severity indices (post-NBR and dNBR) and three UAV severity indicators (percent green fraction, percent green fraction above 5 m, and percent char fraction).

Figure 4 shows the scatterplots, best-fit exponential equations and lines, coefficients of determination (R^2), and root mean squared errors (RMSE) for these six modeled relationships. The post-NBR showed stronger relationships with both the green tree fraction (Figure 4b; Adjusted R^2 = 0.81) and char fraction (Figure 4c; Adjusted R^2 = 0.79), while the dNBR was more closely related to the total green fraction

(Figure 4d; Adjusted R^2 = 0.69). Initial visualizations of the scatterplots in Figure 4 may suggest that there is a possible pattern of increasing residual error with changing post-NBR or dNBR values, but standardized residual plots proved otherwise. Example standardized residual plots for Figure 4e,f, where this pattern appeared most obvious, do not depict a pattern of increasing variance across the range of dNBR (Figure 5a,b, respectively). The Wilcoxin signed-rank test also showed no statistical differences ($p > 0.05$) in the predicted versus actual green and char fractions from the 30% validation sample ($n = 167$), when these were predicted using the models developed from the 70% training sample ($n = 388$) (Table 3). However, green tree fraction predictions were statistically different ($p < 0.05$) from either Landsat predictor (Table 3).

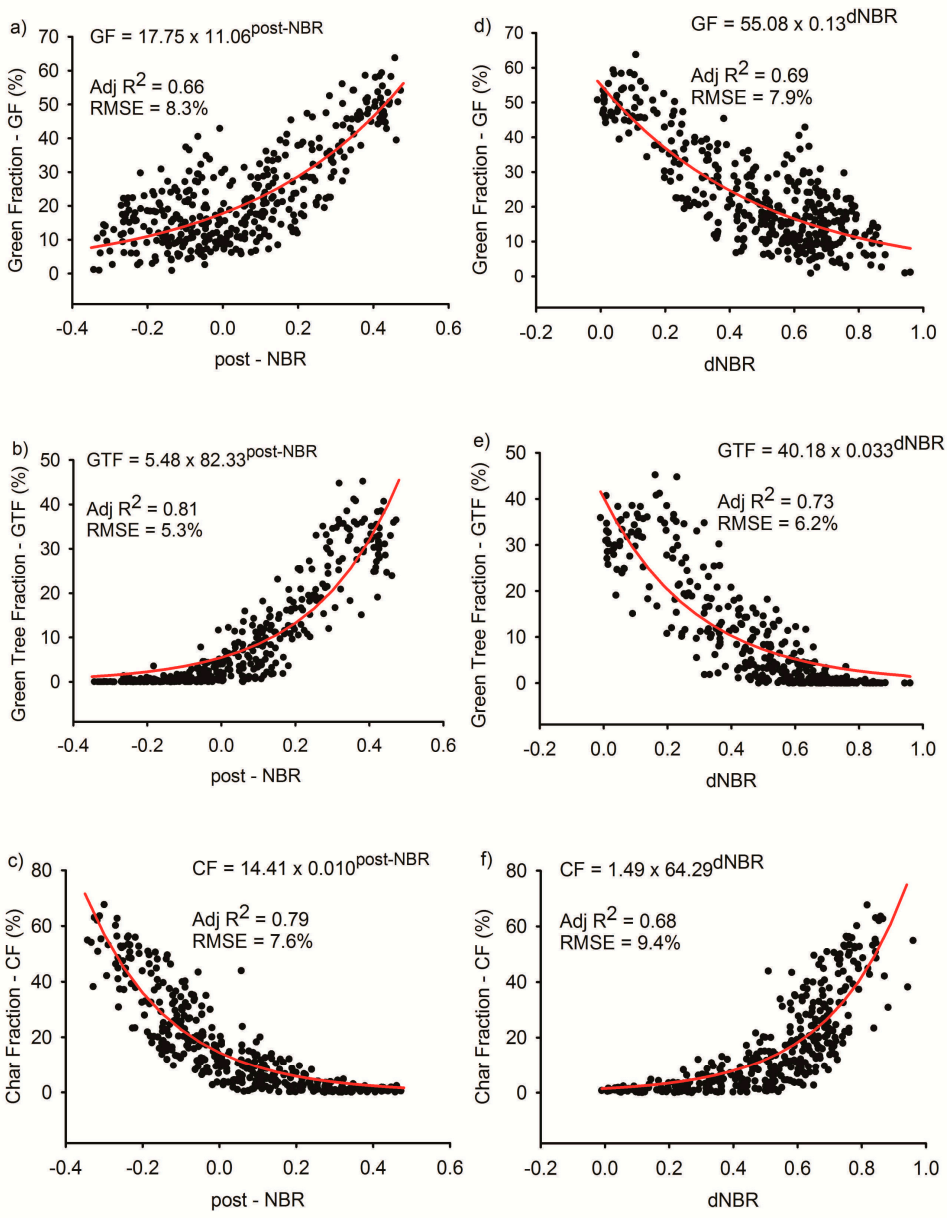

Figure 4. Scatterplots showing the relationships between the post-NBR and dNBR Landsat severity indices (*x*-axes) and three UAV-based severity indicators (*y*-axes), aggregated within the 30 m resolution Landsat pixel footprints. The best-fit exponential regression lines and equations are also shown for each relationship. The individual plots are post-NBR vs. green fraction (**a**), post-NBR vs. green tree fraction (**b**), post-NBR vs. char fraction (**c**), dNBR vs. green fraction (**d**), dNBR vs green tree fraction (**e**), and dNBR vs. char fraction (**f**).

Table 3. Test predictions for statistical differences (p = 0.05) from non-linear models employing independent validation samples using a Wilcoxin signed-rank test.

Landsat Severity Index (*X*)	UAV Measure of Severity (*Y*)	*p*-Values
post-NBR	Green Fraction	0.74
	Green Tree Fraction	0.00
	Char Fraction	0.29
dNBR	Green Fraction	0.93
	Green Tree Fraction	0.00
	Char Fraction	0.28

Non-linear models for predicting the overall CBI using the Landsat indices and UAV severity indicators are summarized in Table 4. The post-NBR and dNBR Landsat indices could explain similar amounts of CBI variance (Adjusted R^2 = 0.53–0.59), with relationships that were somewhat weaker (Adjusted R^2 = 0.82–0.85) than those reported in [16], based on dNBR. The results also indicated the UAV green fraction indices were comparable to the Landsat indices in their ability to predict the CBI.

Table 4. Best fit non-linear models for predicting the overall CBI using the Landsat and UAV severity indices.

Overall CBI Predictor	Non-Linear Model *Y* = Overall CBI	Adj R^2	RMSE
Landsat indices			
post-NBR	Ln (9.47–20.74 post-NBR)	0.59	0.60
dNBR	3.20 $dNBR^{0.63}$	0.53	0.64
UAV indices			
Green Fraction (GF)	2.60–1.16 GF^2	0.52	0.58
Green Tree Fraction (GTF)	2.70×0.96^{GTF}	0.60	0.54
Char Fraction (CF)	Ln (3.81–0.29 post-NBR)	0.36	0.67

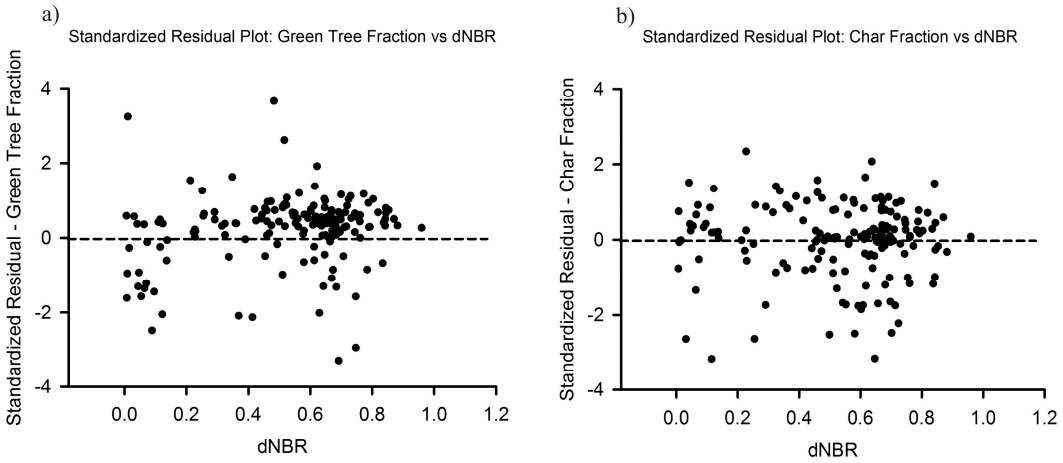

Figure 5. Standardized residual plots derived from the fitted relationships shown in Figure 4e (**a**) and Figure 4f (**b**) depicting no bias and a homogeneous pattern across the range of dNBR.

4. Discussion

Previous studies of boreal forest burn severity have shown that the Landsat dNBR index generally demonstrates the strongest relationship to the field-based CBI designed to measure overall burn severity [21]. The NBR exhibits a large drop after burning, owing to the removal of leafy vegetation,

which decreases NIR scattering, SWIR water absorption and canopy shadowing [22,45]. In this study, we similarly found that dNBR was effective for predicting CBI (Table 4), but also demonstrated that Landsat indices were even more closely related to specific indicators of burn severity derived from UAV mapping (Figure 4). The post-NBR and dNBR indices could each explain a similar amount of the variation in the UAV-derived green vegetation fraction, while the post-NBR was a better predictor of the UAV char fraction. These Landsat-UAV relationships are consistent with [38], where Landsat severity indices were most highly correlated to the green crown fraction and total charred ground surface from a set of 32 fire effect field measures from Alaska.

It is important to note that the strongest modeled relationship was for the UAV green tree fraction predicted using the post-NBR (Figure 4b). Despite the strength of this relationship, the high degree of flattening at low post-NBR values makes it relatively less useful as a means to calibrate the NBR, compared to the total green fraction or char fraction relationships. The major reason for this is that the large proportion of crown fire within our study sites led to a majority (57%) of 30 m Landsat pixels containing less than five percent green tree crown (Figure 6, FP15_21). As a result, this UAV indicator had a relatively minor influence on 30 m post-NBR values over most of the post-NBR range.

Superimposing a raster of the regression model residuals over the UAV orthomosaic can provide insight into the specific reasons for scattering in the model results shown in Figure 4. An examination of the residuals for the first plot (post-NBR vs. green fraction) shows that values are often spatially clumped, rather than random. While there don't appear to be consistent causes for either model over- or under-prediction of the UAV green fraction, some patterns are apparent. For example, some areas where the actual UAV-derived green fraction is higher than the Landsat-predicted fraction (i.e., underestimation) are associated with relatively open and unburned canopies that contain fewer shadows, which may otherwise obscure unburned ground vegetation (Figure 6, FP15_20). This can result in a higher UAV-mapped green fraction compared to areas where shadows obscure more of the ground surface. By contrast, some areas where the actual green fraction is lower than the amount predicted (i.e., overestimation) correspond to standing scorched tree canopies with brown/orange needles (Figure 6, FP15_19), or with a ground layer of dropped needles (Figure 6, FP_22). These canopies encountered a less severe fire at the surface and lower canopy strata, but it was severe enough to scorch the needles through proximal heating, without direct flame contact. The Jenks classifier was used to create a binary, burned versus green vegetation classification, whereby scorched crowns were not treated as a separate, less severe vegetation response class.

Most Landsat-based studies of boreal burn severity have applied the dNBR, which is a bi-temporal index representing spectral changes from pre- to post-fire conditions [16,21,27,28]. However, investigations in Alaska, where black spruce is the predominant tree species, have shown that the post-NBR can be more highly correlated than the dNBR to field-measured fire effects [29,38,46]. The choice of a uni- or multi-temporal index to characterise severity should be based primarily on the accuracy for measuring fire effects, but may also reflect other considerations. For example, an index that measures spectral changes such as the dNBR, should be theoretically preferable for studies of burn severity, since, by definition, this term describes the degree of ecosystem change resulting from fire. The CBI, which was developed as a field measure of severity for calibrating dNBR, is similarly based on ecological changes, although pre-fire conditions must often be inferred [22,23]. A bi-temporal index also permits a more accurate mapping of the extent of burning (a pre-requisite for determining severity), by avoiding commission errors over unvegetated areas that can result from only using a post-fire index. In our study, the post-NBR and dNBR were comparable in their ability to predict UAV-based green vegetation fractions, while the post-NBR was a better predictor of the UAV char fraction. The better performance of the post-NBR may be due, in part, to the char indicator having little or no dependence on the pre-burn conditions that influence the dNBR values. The inclusion of a pre-burn NBR to generate the dNBR has the potential to add spectral variability unrelated to fire, due to image differences in solar illumination, atmosphere, phenology, and spatial registration [31,47], or differences in the pre-fire forest condition [48]. Based on these results, a potential strategy for upscaling

the UAV indicators using Landsat imagery may be to use the dNBR for mapping the extent of fires and green vegetation fractions, followed by the post-NBR to estimate char fractions.

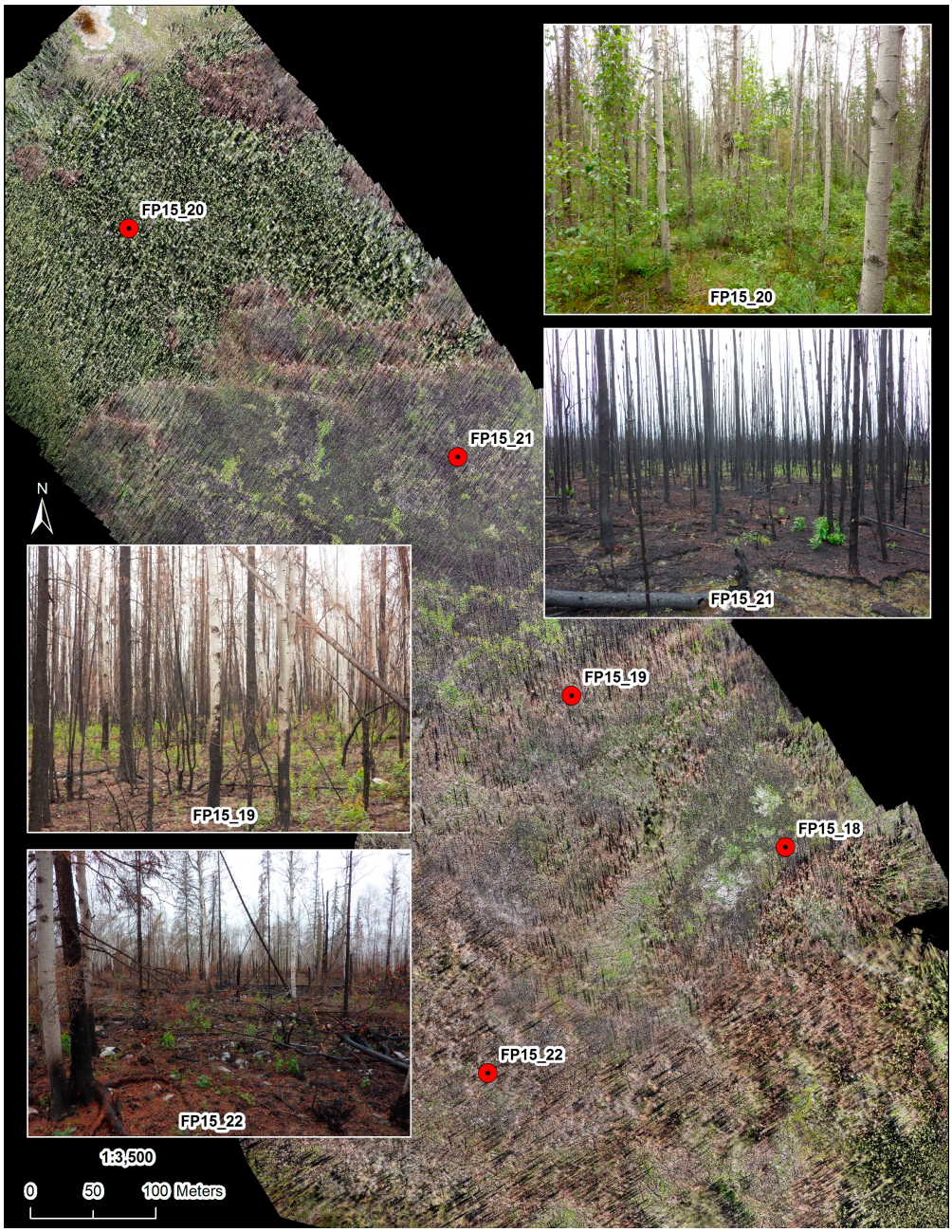

Figure 6. Portion of the UAV orthmosaic for study area #1 (centered at 69.905°N, 116.53°W), showing the locations of four CBI plots with corresponding inset ground photos.

The strong relationship between the dNBR/post-NBR and the UAV-derived severity indicators, permits the translation of the Landsat indices into measures of burn severity with a greater biophysical underpinning. Figure 7 shows the pre- and post-fire Landsat image and predicted residual green vegetation and char fractions based on the NBR-UAV non-linear regression functions, for a larger 60 km^2 area within our study region. Considering the diversity of the fuel types sampled (Table 1) and the results from the hold-out validation sample, these regression relationships should be applicable to other areas within in the post-burn Landsat image that burned under similar conditions. However, the

relationships may not be valid for other images captured at different post-fire regeneration intervals, and should also be tested for their extendibility over a wider range of forest ecological conditions [16,21].

The area of charred surface was derived from UAV mapping to indicate the extent of burning in the surface organic layer. A second potentially useful metric of surface burning not investigated here, is the presence of light coloured ash, which indicates that the fire has completely combusted organic material, such as large woody debris. The amount of ash cover has been related to surface fuel consumption in the boreal forest [19,49], and could thus provide a valuable UAV-based measure of burn severity in the surface layer. The extent of light ash could potentially be derived using a colour index similar to our Char Index, but by identifying a bright, rather than dark, colourless surface. However, note that ash, unlike char, could be challenging to separate from other surfaces such as bright rock, based on colour alone. A very high resolution digital surface model derived from UAV photogrammetry and/or image segmentation techniques could potentially assist with this [39]. Ash cover can also be rapidly removed by wind and rainfall, so UAV surveys may need to be conducted relatively soon after burning. The mapping of light ash would be a more important consideration for boreal burns containing larger proportions of ash than were encountered in our study sites [50], and where it would be more likely to influence Landsat burn indices at a 30 m scale [42].

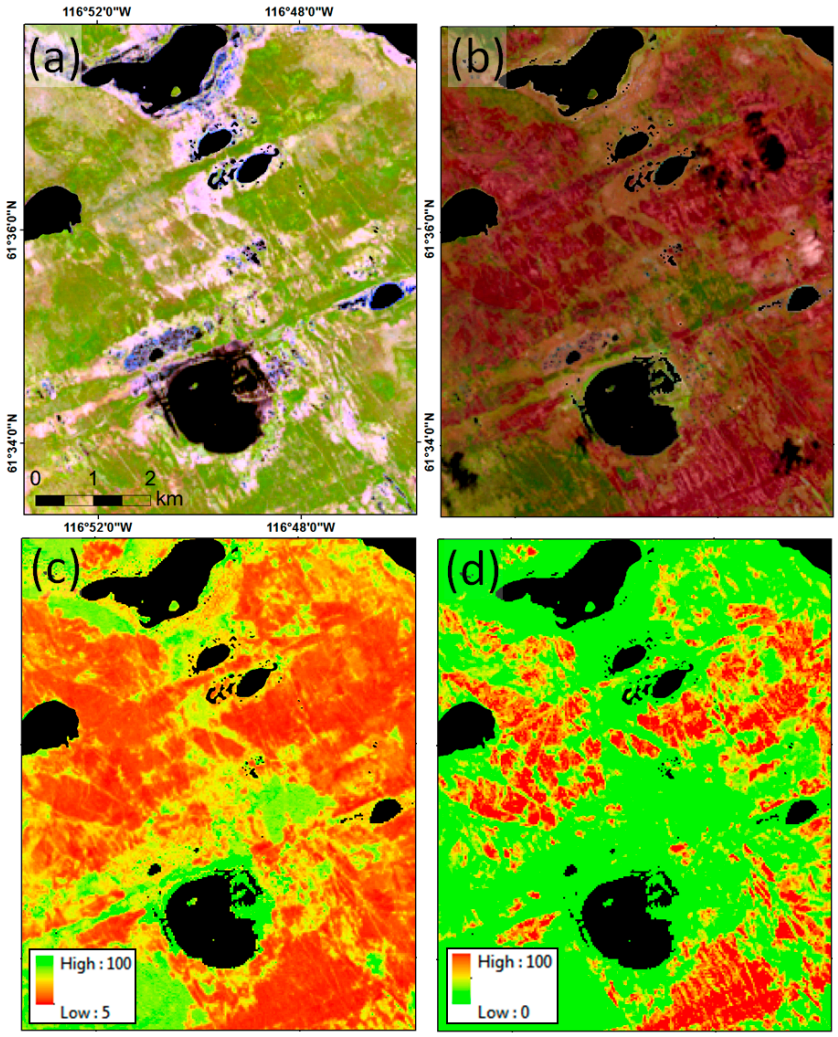

Figure 7. A 60 km^2 area within our study region captured using (**a**) pre-burn Landsat-8 imagery from 17 July 2013; and (**b**) post-burn Landsat-8 imagery from 23 July 2015 (RGB = SWIR, NIR, Red); Predictions of percent post-burn green vegetation cover and percent charred surface cover, based on UAV calibration of Landsat burn indices, are shown respectively in (**c**,**d**).

In this study we made limited use of the UAV-based vegetation height model to separate the portion of residual green vegetation that lies above 5 m in the tree canopy. A vegetation height model could be further exploited to stratify UAV severity metrics according to the five CBI height classes, in an attempt to mimic specific factors that form the overall CBI rating. UAV-based colour and height information could also be investigated, to quantify more complex indicators of burn severity, including the area of scorched needle-leaf crowns, char height [51], density of standing and downed boles with no foliage, and the presence of exposed mineral soil arising from the complete combustion of surface organic material. The calculation of these metrics may require higher resolution UAV photos with a larger overlap than those collected in this study [39], to facilitate characterizing the detailed structure of residual dead and living trees. The goal of follow-on research should therefore focus on a more comprehensive UAV-based protocol for plot-scale assessments of burn severity, which could include select field-measured attributes, such as depth of surface burning [15,17], that may be difficult to address using UAV photogrammetry alone. If successful, the major advantage of such a hybrid protocol would be the ability to conduct more quantitative, repeatable, and objective burn severity assessments with a closer physical linkage to satellite-based indices, to allow for robust up-scaling.

Some other potential applications of UAV-based, SfM modeling for studying boreal fires include: (1) providing reference data for training and validating burned area mapping algorithms that use Landsat's or higher resolution satellite sensors; (2) mapping the charred standing bole density to help guide post-fire salvage logging efforts; and (3) quantifying long-term regeneration rates and structural changes in recovering burned forest, similar to previous studies that have used LiDAR [20]. Because of the relatively limited extents that can be surveyed using UAVs, relative to manned aircraft or satellite-based sensors, these applications would have to examine sites that had been carefully chosen to represent larger-area conditions.

Finally, the development of UAV-based burn severity indices in this study was not without certain limitations and challenges. Here we highlight several:

(1) Our surveys were conducted under clear, sunny conditions that caused strong shadows to cover much of the ground in areas with dense residual tree cover. Shadowing could be minimized by conducting surveys in light, overcast conditions.
(2) Surface char was completely obscured in some areas, due to a dense layer of scorched conifer needles that dropped from the above canopy.
(3) We did not validate the accuracy of the tree canopy height model and assumed that it was sufficiently accurate for broadly separating ground-level vegetation and tree crowns that lie above 5 m. For reference, Wallace et al. [52] created UAV/SfM-based canopy height models that could estimate 4.7–16.2 m eucalyptus tree heights, with a root mean square error of 1.3 m.
(4) The binary Jenks classifier, used for separating both green vegetation and shadows, was found to be simple and effective, yet may not be as accurate as more advanced classifiers or those that include a third, less severe vegetation response class for brown/orange scorched canopies.
(5) A rigorous validation of very high resolution, UAV-derived indicators of burn severity is challenging, because of the requirement to collect reference data that is at least as detailed and spatially precise. The approach used in this study for mapping green vegetation and char was to relate photo-interpreted conditions, based on ground and UAV photos, to a georeferenced UAV orthomosaic. However, the validation of more advanced and structural measures of burn severity from UAV photogrammetry will require precisely georeferenced field-based measurements.
(6) We used a consumer-grade RGB camera mounted on a UAV to capture images in JPEG format, that provided simple digital number intensity values. Note that such data have an unknown relationship to scene radiance [53], and would be impacted by any changes in solar illumination during a survey. While we found that such imagery is suitable for separating broad and distinct classes, such as green vegetation and charred surface, more detailed vegetation characterization could benefit from using miniaturized multi- or hyper-spectral instruments that

provide additional spectral information, and where radiance is normalized based on incident light sensors. Note, however, that such sensors currently provide coarser pixel resolutions (e.g., 1–2 megapixels) that may make the SfM modeling of a tree structure challenging.

5. Conclusions

Our results demonstrate that UAV-based photographic surveys and SfM processing methods can provide cost-effective, georeferenced information related to two basic indicators of boreal forest burn severity: the fraction of green vegetation, which includes both residual and regenerating plants, and the fraction of charred organic surfaces. These indicators were highly related to Landsat spectral indices (dNBR and post-NBR) commonly used to assess burn severity, which then permits assigning a biophysical scale to these indices at regional levels. We also found that the UAV severity metrics were similarly correlated to the plot-based CBI, compared to Landsat indices. The operational flexibility of UAVs ensures that mapping can be timed to closely match the acquisition of Landsat satellite imagery used in an extended post-burn assessment. Follow-on research will investigate additional, more complex measures of burn severity that make greater use of a vegetation height model to characterize the post-burn vegetation structure.

Acknowledgments: We thank Rob Skakun from the Canadian Forest Service and Kathleen Groenewegen from the Government of Northwest Territories for assisting with collecting CBI plot data, Kathleen Groenewegen for providing forest inventory data, and Ian Olthof from CCRS for assistance in processing the Landsat imagery. Tim Lynham and Ian Olthof provided helpful comments to improve the manuscript. This work was supported by Polar Knowledge Canada and NRCan's TRACS project led by Stephen Wolfe.

Author Contributions: Robert H. Fraser and Jurjen van der Sluijs conceived the study,and acquired and processed the datasets; Robert H. Fraser led the spatial data analysis and wrote the first draft of the manuscript; Ronald J. Hall led the statistical analysis; and all authors were responsible for the research design, interpreting the results, and the writing and editing of the manuscript.

Conflicts of Interest: The authors declare no conflict of interest.

References

1. Kasischke, E.S.; Turetsky, M.R. Recent changes in the fire regime across the North American boreal region—Spatial and temporal patterns of burning across Canada and Alaska. *Geophys. Res. Lett.* **2006**, *33*, L09703. [CrossRef]
2. Kurz, W.A.; Stinson, G.; Rampley, G.J.; Dymond, C.C.; Neilson, E.T. Risk of natural disturbances makes future contribution of Canada's forests to the global carbon cycle highly uncertain. *Proc. Natl. Acad. Sci. USA* **2008**, *105*, 1551–1555. [CrossRef] [PubMed]
3. McCullough, D.G.; Werner, R.A.; Neumann, D. Fire and insects in northern and boreal forest ecosystems of North America. *Annu. Rev. Entomol.* **1998**, *43*, 107–127. [CrossRef] [PubMed]
4. Kurz, W.A.; Shaw, C.H.; Boisvenue, C.; Stinson, G.; Metsaranta, J.; Leckie, D.; Dyk, A.; Smyth, C.; Neilson, E.T. Carbon in Canada's boreal forest—A synthesis. *Environ. Rev.* **2013**, *21*, 260–292. [CrossRef]
5. Amiro, B.D.; Todd, J.B.; Wotton, B.M.; Logan, K.A.; Flannigan, M.D.; Stocks, B.J.; Mason, J.A.; Martell, D.L.; Hirsch, K.G. Direct carbon emissions from Canadian forest fires, 1959–1999. *Can. J. For. Res.* **2001**, *31*, 512–525. [CrossRef]
6. Thomas, D.C.; Barry, S.J.; Alaie, G. Fire-caribou-winter range relationships in northern Canada. *Rangifer* **1996**, *16*, 57–67. [CrossRef]
7. Burn, C.R. The response (1958–1997) of permafrost and near-surface ground temperatures to forest fire, Takhini River Valley, Southern Yukon Territory. *Can. J. Earth Sci.* **1998**, *35*, 184–199. [CrossRef]
8. Amiro, B.D.; Cantin, A.; Flannigan, M.D.; de Groot, W.J. Future emissions from Canadian boreal forest fires. *Can. J. For. Res.* **2009**, *39*, 383–395. [CrossRef]
9. Johnston, M.; Williamson, T.; Munson, A.; Ogden, A.; Moroni, M.; Parsons, R.; Price, D.; Stadt, J. *Climate Change and Forest Management in Canada: Impacts, Adaptive Capacity and Adaptation Options*; A State of Knowledge Report; Sustainable Forest Management Network: Edmonton, AB, Canada, 2010; p. 54.

10. Price, D.T.; Alfaro, R.I.; Brown, K.J.; Flannigan, M.D.; Fleming, R.A.; Hogg, E.H.; Girardin, M.P.; Lakusta, T.; Johnston, M.; McKenney, D.W.; et al. Anticipating the consequences of climate change for Canada's boreal forest ecosystems. *Environ. Rev.* **2013**, *21*, 322–365. [CrossRef]
11. Lentile, L.B.; Holden, Z.A.; Smith, A.M.S.; Falkowski, M.J.; Hudak, A.T.; Morgan, P.; Lewis, S.A.; Gessler, P.E.; Benson, N.C. Remote sensing techniques to assess active fire characteristics and post-fire effects. *Int. J. Wildland Fire* **2006**, *15*, 319–345. [CrossRef]
12. Macdonald, S.E. Effects of partial post-fire salvage havesting on vegetation communities in the boreal mixedwood forest region of northeastern Alberta, Canada. *For. Ecol. Manag.* **2007**, *239*, 21–31. [CrossRef]
13. Johnstone, J.F.; Chapin, F.S., III. Effects of soil burn severity on post-fire tree recruitment in boreal forest. *Ecosystems* **2006**, *9*, 14–31. [CrossRef]
14. Smucker, K.M.; Hutto, R.L.; Steele, B.M. Changes in bird abundance after wildfire: Importance of fire severity and time since fire. *Ecol. Appl.* **2005**, *15*, 1535–1549. [CrossRef]
15. Kasischke, E.S.; Johnstone, J.F. Variation in postfire organic layer thickness in a black spruce forest complex in interior Alaska and its effects on soil temperature and moisture. *Can. J. For. Res.* **2005**, *35*, 2164–2177. [CrossRef]
16. Hall, R.J.; Freeburn, J.T.; de Groot, W.J.; Pritchard, J.M.; Lynham, T.J.; Landry, R. Remote sensing of burn severity: Experience from western Canada boreal fires. *Int. J. Wildland Fire* **2008**, *17*, 476–489. [CrossRef]
17. Boby, L.A.; Schuur, E.A.G.; Mack, M.C.; Verbyla, D.; Johnstone, J.F. Quantifying fire severity, carbon, and nitrogen emissions in Alaska's boreal forest. *Ecol. Appl.* **2010**, *20*, 1633–1647. [CrossRef] [PubMed]
18. Routledge, R.G. *Sampling Methodology for Studying Boreal Postfire Residual Stand Structure with High Resolution Aerial Photography and Field Plots*; Forest Research Information Paper No. 169; Ontario Forest Research Institute: Sault Ste. Marie, ON, Canada, 2007.
19. Lewis, S.A.; Hudak, A.T.; Ottmar, R.D.; Robichaud, P.R.; Lentile, L.B.; Hood, S.M.; Cronan, J.B.; Morgan, P. Using hyperspectral imagery to estimate forest floor consumption from wildfire in boreal forests of Alaska, USA. *Int. J. Wildland Fire* **2011**, *20*, 255–271. [CrossRef]
20. Magnussen, S.; Wulder, M.A. Post-fire canopy height recovery in Canada's boreal forests using Airborne Laser Scanner (ALS). *Remote Sens.* **2012**, *4*, 1600–1616. [CrossRef]
21. French, N.H.F.; Kasischke, E.S.; Hall, R.J.; Murphy, K.A.; Verbyla, D.L.; Hoy, E.E.; Allen, J.L. Using Landsat data to assess fire and burn severity in the North American boreal forest region: An overview and summary of results. *Int. J. Wildland Fire* **2008**, *17*, 443–462. [CrossRef]
22. Key, C.H.; Benson, N.C. Landscape assessment: Sampling and analysis methods. In *FIREMON: Fire Effects Monitoring and Inventory System*; Lutes, D.C., Keane, R.E., Caratti, J.F., Key, C.H., Benson, N.C., Sutherland, S., Gangi, L.H., Eds.; General Technical Report 164; USDA Rocky Mountain Research Station: Fort Collins, CO, USA, 2006; pp. LA1–LA51.
23. Morgan, P.; Keane, R.E.; Dillon, G.K.; Jain, T.B.; Hudak, A.T.; Karau, E.C.; Sikkink, P.G.; Holden, Z.A.; Strand, E.K. Challenges of assessing fire and burn severity using field measures, remote sensing and modelling. *Int. J. Wildland Fire* **2014**, *23*, 1045–1060. [CrossRef]
24. Kasischke, E.S.; Turetsky, M.R.; Ottmar, R.D.; French, N.H.F.; Hoy, E.E.; Kane, E.S. Evaluation of the composite burn index for assessing fire severity in Alaskan black spruce forests. *Int. J. Wildland Fire* **2008**, *17*, 515–526. [CrossRef]
25. Chu, T.; Guo, X. Remote sensing techniques in monitoring post-fire effects and patterns of forest recovery in boreal forest regions: A review. *Remote Sens.* **2013**, *6*, 470–520. [CrossRef]
26. Wing, M.G.; Burnett, J.D.; Sessions, J. Remote sensing and unmanned aerial system technology for monitoring and quantifying forest fire impacts. *Int. J. Remote Sens. Appl.* **2014**, *4*, 18. [CrossRef]
27. Soverel, N.O.; Perrakis, D.D.B.; Coops, N.C. Estimating burn severity from Landsat dNBR and RdNBR indices across western Canada. *Remote Sens. Environ.* **2010**, *114*, 1896–1909. [CrossRef]
28. Boucher, J.; Beaudoin, A.; Hébert, C.; Guindon, L.; Bauce, É. Assessing the potential of the differenced Normalized Burn Ratio (dNBR) for estimating burn severity in eastern Canadian boreal forests. *Int. J. Wildland Fire* **2016**. [CrossRef]
29. Hoy, E.E.; French, N.H.F.; Turetsky, M.R.; Trigg, S.N.; Kasischke, E.S. Evaluating the potential of Landsat TM/ETM+ imagery for assessing fire severity in Alaskan black spruce forests. *Int. J. Wildland Fire* **2008**, *17*, 500–514. [CrossRef]

30. Murphy, K.A.; Reynolds, J.H.; Koltun, J.M. Evaluating the ability of the differenced Normalized Burn Ratio (dNBR) to predict ecologically significant burn severity in Alaskan boreal forests. *Int. J. Wildland Fire* **2008**, *17*, 490–499. [CrossRef]
31. Verbyla, D.L.; Kasischke, E.S.; Hoy, E.E. Seasonal and topographic effects on estimating fire severity from Landsat TM/ETM+ data. *Int. J. Wildland Fire* **2008**, *17*, 527–534. [CrossRef]
32. Whitehead, K.; Hugenholtz, C.H. Remote sensing of the environment with small unmanned aircraft systems (UASs), Part 1: A review of progress and challenges. *J. Unmanned Veh. Syst.* **2014**, *2*, 69–85. [CrossRef]
33. Ambrosia, V.G.; Wegener, S.; Zajkowski, T.; Sullivan, D.V.; Buechel, S.; Enomoto, F.; Lobitz, B.; Johan, S.; Brass, J.; Hinkley, E. The Ikhana unmanned airborne system (UAS) western states fire imaging missions: From concept to reality (2006–2010). *Geocarto Int.* **2011**, *26*, 85–101. [CrossRef]
34. Simpson, J.; Wooster, M.; Smith, T.; Trivedi, M.; Vernimmen, R.; Dedi, R.; Shakti, M.; Dinata, Y. Tropical peatland burn depth and combustion heterogeneity assessed using UAV photogrammetry and airborne LiDAR. *Remote Sens.* **2016**, *8*, 1000. [CrossRef]
35. Ecosystem Classification Group. *Ecological Regions of the Northwest Territories—Taiga Plains*; Department of Environment and Natural Resources, Government of the Northwest Territories: Yellowknife, NT, Canada, 2007.
36. Allen, J.L.; Sorbel, B. Assessing the differenced Normalized Burn Ratio's ability to map burn severity in the boreal forest and tundra ecosystems of Alaska's national parks. *Int. J. Wildland Fire* **2008**, *17*, 463–475. [CrossRef]
37. Westoby, M.J.; Brasington, J.; Glasser, N.F.; Hambrey, M.J.; Reynolds, J.M. "Structure-from-Motion" photogrammetry: A low-cost, effective tool for geoscience applications. *Geomorphology* **2012**, *179*, 300–314. [CrossRef]
38. Hudak, A.T.; Morgan, P.; Bobbitt, M.J.; Smith, A.M.S.; Lewis, S.A.; Lentile, L.B.; Robichaud, P.R.; Clark, J.T.; McKinley, R.A. The relationship of multispectral satellite imagery to immediate fire effects. *Fire Ecol.* **2007**, *3*, 64–90. [CrossRef]
39. Fraser, R.H.; Olthof, I.; Lantz, T.C.; Schmitt, C. UAV photogrammetry for mapping vegetation in the low-Arctic. *Arct. Sci.* **2016**, *2*, 79–102. [CrossRef]
40. Chander, G.; Markham, B.L.; Helder, D.L. Summary of current radiometric calibration coefficients for Landsat MSS, TM, ETM+, and EO-1 ALI sensors. *Remote Sens. Environ.* **2009**, *113*, 893–903. [CrossRef]
41. Kaufman, Y.J.; Remer, L.A. Detection of forests using mid-IR reflectance: An application for aerosol studies. *IEEE Trans. Geosci. Remote Sens.* **1994**, *32*, 672–683. [CrossRef]
42. Smith, A.M.S.; Wooster, M.J.; Drake, N.A.; Dipotso, F.M.; Falkowski, M.J.; Hudak, A.T. Testing the potential of multi-spectral remote sensing for retrospectively estimating fire severity in African Savannahs. *Remote Sens. Environ.* **2005**, *97*, 92–115. [CrossRef]
43. Hugenholtz, C.; Brown, O.; Walker, J.; Barchyn, T.; Nesbit, P.; Kucharczyk, M.; Myshak, S. Spatial accuracy of UAV-derived orthoimagery and topography: Comparing photogrammetric models processed with direct geo-referencing and ground control points. *Geomatica* **2016**, *70*, 21–30. [CrossRef]
44. Conover, W.J. *Practical Nonparametric Statistics*, 3rd ed.; Wiley Series in Probability and Statistics; John Wiley & Sons, Inc.: New York, NY, USA, 1999.
45. Fraser, R.; Li, Z. Estimating fire-related parameters in boreal forest using spot vegetation. *Remote Sens. Environ.* **2002**, *82*, 95–110. [CrossRef]
46. Epting, J.; Verbyla, D.; Sorbel, B. Evaluation of remotely sensed indices for assessing burn severity in interior Alaska using Landsat TM and ETM+. *Remote Sens. Environ.* **2005**, *96*, 328–339. [CrossRef]
47. Escuin, S.; Navarro, R.; Fernández, P. Fire severity assessment by using NBR (Normalized Burn Ratio) and NDVI (Normalized Difference Vegetation Index) derived from LANDSAT TM/ETM images. *Int. J. Remote Sens.* **2008**, *29*, 1053–1073. [CrossRef]
48. McCarley, T.R.; Kolden, C.A.; Vaillant, N.M.; Hudak, A.T.; Smith, A.M.S.; Wing, B.M.; Kellogg, B.S.; Kreitler, J. Multi-temporal LiDAR and Landsat quantification of fire-induced changes to forest structure. *Remote Sens. Environ.* **2017**, *191*, 419–432. [CrossRef]
49. Hudak, A.T.; Ottmar, R.D.; Vihnanek, R.E.; Brewer, N.W.; Smith, A.M.S.; Morgan, P. The relationship of post-fire white ash cover to surface fuel consumption. *Int. J. Wildland Fire* **2013**, *22*, 780–785. [CrossRef]
50. Bourgeau-Chavez, L.L.; French, N.H.F.; Endres, S.; Jenkins, L.; Battaglia, M.; Serocki, E.; Billmire, M. *ABoVE: Burn Severity, Fire Progression, Landcover and Field Data, NWT, Canada, 2014*; ORNL DAAC: Oak Ridge, TN, USA, 2016.

51. Hély, C.; Flannigan, M.; Bergeron, Y. Modeling tree mortality following wildfire in the Southeastern Canadian mixed-wood boreal forest. *For. Sci.* **2003**, *49*, 566–576.
52. Wallace, L.; Lucieer, A.; Malenovský, Z.; Turner, D.; Vopěnka, P. Assessment of forest structure using two UAV techniques: A comparison of airborne laser scanning and structure from motion (SfM) point clouds. *Forests* **2016**, *7*, 62. [CrossRef]
53. Akkaynak, D.; Treibitz, T.; Xiao, B.; Gürkan, U.A.; Allen, J.J.; Demirci, U.; Hanlon, R.T. Use of commercial off-the-shelf digital cameras for scientific data acquisition and scene-specific color calibration. *J. Opt. Soc. Am. A Opt. Image Sci. Vis.* **2014**, *31*, 312–321. [CrossRef] [PubMed]